doi: 10.82124/CEAS-GNC-2026-081 CEAS-GNC-2026-081

Oscillatory control of rocket thrust vector for unthrottled powered precision landing

Maciej Michałów PhD student, ISAE-SUPAERO, Université de Toulouse 1, Toulouse, France. maciej.michalow@isae-supaero.fr

Daniel Alazard Professor, Fédération ENAC ISAE-SUPAERO ONERA, Université de Toulouse, Toulouse, France. daniel.alazard@isae-supaero.fr

Leandro Ribeiro Lustosa Associate professor, Fédération ENAC ISAE-SUPAERO ONERA, Université de Toulouse, France. leandro.ribeiro-lustosa@isae-supaero.fr

ABSTRACT

Reusable launchers and landers usually rely on throttling and thrust vector control (TVC) during the terminal phase of their descent. Since throttling is the only direct way of controlling the descent speed, it might seem indispensable for a soft precision landing. This would preclude the use of solid rocket propulsion in both classes of spacecraft and render a throttling malfunction virtually unrecoverable due to lack of controllability, unless sophisticated trajectory generation techniques were employed. In contrast, this paper demonstrates that an unthrottled lander remains fully locally controllable from both a theoretical and practical point of view. First, nonlinear controllability is shown parametrically using Lie bracket analysis. Next, a practical way to achieve this full controllability is proposed, using oscillatory TVC to modulate mean thrust while retaining independent control of the attitude and lateral axis, as demonstrated by analyzing the average dynamics. A linear state feedback controller is proposed to stabilize the resulting system, with closed-loop stability demonstrated numerically for both the average dynamics (using linearization and eigenvalues) and for the full time-dependent system (using Floquet theory). The practical performance of the control architecture is demonstrated in an example spacecraft performing a landing maneuver. The practical limitations of the oscillatory control scheme are then discussed, especially with regard to the bounds on mean thrust control authority and the practical limitations of the oscillation frequency.

Keywords: reusable launchers, oscillatory control, averaging theory, underactuated systems, thrust vector control

Nomenclature

$\star$	=	expression which is nonzero at $\mathbf{x}_{\text{eq}}$
$\dagger$	=	nonzero expression equal to 0 at $\mathbf{x}_{\text{eq}}$
$\bar{\cdot}$	=	function or value averaged over t or relating to average dynamics
$\tilde{\cdot}$	=	dynamical value relating to thema system in control-affine form
$\dot{(\cdot)}$	=	derivative with respect to t
$(\cdot)'$	=	derivative with respect to τ
$(\cdot)_{\text{cl}}$	=	signal relating to system in closed-loop

$(\cdot)_{\text{eq}}$ = value at equilibrium
$(\cdot)_{\text{max}}$ = maximum value
$(\cdot)_{\text{min}}$ = minimum value
$(\cdot)_{\text{osc}}$ = signal relating to system under oscillatory control
$(\cdot)_{\text{sf}}$ = signal relating to state feedback
$(\cdot)_{\text{sp}}$ = setpoint of a controlled variable
$[\cdot, \cdot]$ = Lie bracket of two vector fields
Δ = amplitude of δ oscillations
ΔT = thrust increment due to oscillatory control
$\Delta \mathbf{x}$ = state increment with respect to periodic orbit
$\Delta \mathbf{x}_{\Pi}^{(i)}$ = near-periodic trajectory with i-th coordinate perturbed
Π = period of δ oscillations
γ = gravitational acceleration
δ = thrust vector angle
ν = frequency of δ oscillations (analogous to ω)
ϵ = small positive number
ζ_{a} = damping factor of the TVC actuator
θ = pitch angle
τ = time normalized with respect to ω
$\boldsymbol{\phi}$ = state evolution function
ω = angular frequency of δ oscillations (analogous to ν)
ω_{a} = natural frequency of the TVC actuator
$\mathbf{A}$ = state transition matrix
$\mathbf{B}$ = input matrix
$\boldsymbol{C}$ = Kalman controllability matrix
J = moment of inertia along pitch axis
$\mathbf{K}$ = feedback gain matrix
$\boldsymbol{\mathcal{L}}$ = matrix of nested Lie brackets
$\boldsymbol{\mathcal{M}}$ = monodromy matrix
$\mathbf{Q}$ = state error LQR cost matrix
$\mathbf{R}$ = input LQR cost matrix
a = Δ-dependent constant
b = Δ-dependent constant
c = Δ-dependent constant
$\mathbf{e}_i$ = unit vector with i-th non-zero component
$\mathbf{f}$ = drift term of system dynamics
$\mathbf{g}$ = input term of system dynamics
k = number of inputs
l = lever arm of thrust with respect to CG
m = mass
n = number of states
p_x = position along x axis
p_z = position along z axis
q = angular rate
$\mathbf{r}$ = time-independent part of $\mathbf{f}$
$\mathbf{s}$ = time-dependent part of $\mathbf{f}$
t = time
u = input signal
v_x = velocity along x axis
v_z = velocity along z axis

$\mathbf{x}$ = state vector
$\mathbf{x}_\Pi$ = periodic orbit

1 Introduction

1.1 Control of landing rockets

Over the last decade, reusable landing rockets have progressed from initial proof-of-concept demonstrations to an extensively flight-proven and economically viable solution. As with any innovative technology, once the main objective (controlled soft landing, in this case) has been proven to be feasible and mastered sufficiently for commercial operations, the next steps in the maturation process of the technology include increasing reliability (e.g. the progress in aviation safety from the early Jet Age up to this day) and advances in hardware affordability enabling more mass-scale, low-cost applications (e.g. the development of cheap recreational drones over the last decade). This paper discusses a control mechanism for reusable launchers and landers with possible impact in both categories: retention of full controllability in case of engine throttling failure, and, by extension, precision landing using a non-throttleable solid rocket motor.

A typical landing rocket platform uses up to 4 different sources of actuation in order to achieve controlled landing:

1) **Aerodynamic surfaces** – generate significant control forces, but only during atmospheric descent, when both airspeed and air density are sufficiently high (since aerodynamic forces are proportional to dynamic pressure).
2) **Cold gas thrusters** – useful for attitude adjustments during both exoatmospheric flight and the terminal landing phase; however, they generate very modest forces and rely on limited propellant to operate.
3) **Engine throttling** – by far the most significant mechanism of vertical control.
4) **Thrust vector control (TVC)** – the key source of lateral control in the final landing approach.

The landing rocket is therefore a fully actuated, often even overactuated system. This means that at least some actuator failures should be possible to compensate using alternative control inputs. Attitude and lateral movement can be controlled by many combinations of inputs from of cold gas thrusters, TVC and aerodynamic surfaces; moreover, in the case of rockets with a cluster of multiple engines, antisymmetric differential throttling can also produce a pitching moment. However, for vertical control, options are far more limited. Aside from throttling, which is clearly the principal mechanism, the only alternatives are the drag from the aerodynamic surfaces (which can only provide upwards acceleration, but not nearly enough to compensate for gravity, especially during the terminal phase when airspeed is low) and, only in clustered engine configurations, a net thrust reduction which can be obtained by a symmetric deflection of TVC systems of engines placed symmetrically with respect to the rocket axis (however, it results in structural loads on the rocket and requires care if thrust levels in the engines concerned are not equal). The question arises: for systems without strong aerodynamic control and without multiple clustered engines, is unthrottled precision landing possible at all? This question is relevant for single-engine landing rockets and extraterrestrial landers which either:

1) **undergo a throttling malfunction** – this is a serious concern, since precision landing usually requires deep throttling (i.e. below 25% of nominal thrust [1, 2]), even down to 10% for lunar landing [3], which is technically challenging if done on a single engine (for clustered engines, de-throttling can be achieved by shutting off multiple engines without necessarily intensively throttling down the rest, as discussed in [2]).

2) **are equipped with a solid rocket motor** – since they are much cheaper and less sophisticated than hybrid and liquid propellant rocket engines, this could lead to interesting low-cost applications, e.g. for cargo delivery. However, since solid motors have no control over their predetermined thrust curve, which is subject to some uncertainties due to manufacturing and ambient conditions, their precision landing control architecture must be able to accommodate deviations from nominal thrust.

Multiple studies have already demonstrated control design for reusable launchers and landers, often numerical optimization techniques to generate a landing trajectory which could be then followed using feedback control [4–6]. [7] analyzed the particular case of a model rocket landing without throttle control, using only a single-engine TVC system. An open-loop soft landing trajectory was sought using nonlinear model predictive control (NMPC). The conclusion was that while a soft landing without throttling is possible, the tradeoff is the loss of control over the exact landing spot. [8] used reinforcement learning to achieve precision landing for a constant-thrust rocket using TVC as the only input. The problem with nonlinear optimization methods is, however, their large computational cost, making real-time implementation difficult, and the open-loop nature of the proposed trajectories, making a feedback controller necessary to follow them in a robust manner. [9] showed an interesting hardware solution for using solid rocket propulsion for precision landing: a solid rocket equipped with a dedicated landing engine with 4 concentric downwards-facing nozzles, with the propellant flow through each one being controlled separately (respecting constraints on total flow to prevent pressure buildup in the combustion chamber). This is somewhat equivalent to having 4 clustered throttleable engines.

1.2 Contributions & structure

This paper provides three main contributions to the state of the art:

1) An analytical proof that an unthrottled landing rocket is fully nonlinearly controllable (as long as its thrust-to-weight ratio is within certain bounds), using concepts from geometric control theory.
2) A framework for attaining this full control authority by means of oscillatory TVC, coupled with a proportional state feedback controller for stabilization, with an analytical expression of the average open- and closed-loop dynamics.
3) A numerical case study of this control scheme along with a demonstration of stability using Floquet analysis.

The paper is structured as follows: the remainder of section 1 introduces the theoretical concepts utilized throughout the paper. Section 2 provides the main analytical contributions of the work, introducing the analyzed system in subsection 2.1 and demonstrating its full nonlinear controllability in subsection 2.2; subsection 2.3 introduces oscillatory control as a means of controlling the linearly uncontrollable vertical axis, beginning with physical intuition and following with averaged open-loop dynamics; subsection 2.4 follows with a proportional state feedback controller that stabilizes the resulting system, with the closed-loop average dynamics being derived in subsection 2.5. Section 3 is a numerical case study of a landing model rocket, introduced in subsection 3.1, with an example landing maneuver demonstrated in subsection 3.2, and closed-loop stability being proved via Floquet analysis in subsection 3.3 along with a discussion of the effects of the oscillation frequency. Section 4 follows with conclusions and propositions of further research.

1.3 Controllability of linear and nonlinear systems

As discussed in subsubsection 2.2.1, an unthrottleable landing rocket is not linearly controllable. However, this does not preclude nonlinear controllability, as will be briefly outlined in this subsection with minimal theoretical background; for a rigorous treatment of the topic, refer to [10]. Consider a linear time-invariant dynamical system of order n:

$$\dot{\mathbf{x}} = \mathbf{A}\mathbf{x} + \mathbf{B}\mathbf{u} \tag{1}$$

The Kalman controllability matrix of this system is given by:

$$\boldsymbol{C} = \begin{bmatrix} \mathbf{B} & \mathbf{AB} & \mathbf{A}^2\mathbf{B} & \cdots & \mathbf{A}^{n-1}\mathbf{B} \end{bmatrix} \tag{2}$$

A classical result in linear control theory is that the system given by (1) is controllable if and only if $\boldsymbol{C}$ is full rank. There exists a nonlinear generalization of this approach: consider a sufficiently smooth time-independent nonlinear dynamical system of order n in control-affine form (with k inputs):

$$\dot{\mathbf{x}} = \mathbf{f}(\mathbf{x}) + \sum_{i=1}^{k} \mathbf{g}_i(\mathbf{x}) u_i \tag{3}$$

The system can be linearized around a point of interest $\mathbf{x}_0$; if the linearized system is controllable, the nonlinear system is also controllable in a neighborhood of $\mathbf{x}_0$ [11]. This is a sufficient condition for local controllability, but it is not necessary. To show a more general framework, first it is necessary to introduce the Lie bracket operator between two vector fields:

$$[\mathbf{f}, \mathbf{g}] = \frac{\partial \mathbf{g}}{\partial \mathbf{x}}\mathbf{f} - \frac{\partial \mathbf{f}}{\partial \mathbf{x}}\mathbf{g} \tag{4}$$

Intuitively, the Lie bracket can be interpreted as the direction of net motion resulting from repeatedly moving by a small amount along one field, and then the other; due to their nonlinearity, this direction can in general be linearly independent from either of them (see [10] for more details). Next, a matrix is constructed by horizontally appending the $\mathbf{g}_i$ terms and iterated Lie brackets of the $\mathbf{g}_i$ terms with each other and with $\mathbf{f}$, omitting terms which are zero or linearly dependent of previous columns:

$$\mathcal{L} = [\,[\mathbf{g}_1, ..., \mathbf{g}_k, [\mathbf{g}_1, \mathbf{g}_2], [\mathbf{f}, \mathbf{g}_1], [\mathbf{f}, [\mathbf{f}, \mathbf{g}_2]], ...] \tag{5}$$

If $\mathcal{L}$ is full rank at a point $\mathbf{x}_0$, the system in (3) is reachable in a neighborhood of $\mathbf{x}_0$. When the method is applied to a linear system (i.e. with $\mathbf{f} = \mathbf{A}\mathbf{x}$ and $\mathbf{g}_i = \mathbf{B}_i$), $\mathcal{L} = \boldsymbol{C}$ is obtained (up to some sign differences), highlighting that this method generalizes the linear analysis. It is important to note that the Lie bracket analysis can yield qualitatively stronger results at a point than the Kalman analysis of the linearized system, since it can incorporate nonlinear effects which linearization omits.

Lie bracket controllability analysis has been used in multiple aerospace applications, notably to find nonlinear dynamic near-stall lift augmentation in unsteady airfoils [12], a related near-stall roll authority augmentation by oscillating aileron and rudder inputs [11] and a general controllability analysis for aircraft [13]. Movement along Lie brackets is usually generated by oscillatory input [10, 14]. The problem is more complicated for systems with drift, although some recent advancements have been made [15].

1.4 Dynamics of periodically forced systems

Since nonlinear controllability is often implemented using oscillatory input [11, 13], the resulting systems become time-dependent, and, more specifically, time-periodic. This is not necessarily detrimental; under some circumstances, periodic open-loop input can stabilize a previously unstable system, as seen in the classical Kapitsa pendulum [16], or, as recently discovered, in insect flight [17]; moreover, [18] has shown that a sinusoidal oscillation of thrust magnitude can, under some conditions, improve

the performance of a rocket. Time-dependency causes the analysis of those systems to become more challenging; however, two mature frameworks exist for rigorous analysis of such systems: averaging and Floquet theory; both are very briefly introduced below, since both have been found useful for the purposes of this paper. Although independently developed and very different in their techniques, both approaches have recently been shown to be profoundly related [19]. The remainder of this subsection is a brief outline of both methods with references to sources with a more rigorous presentation.

1.4.1 Averaging theory

The analysis of a time-periodic system can be made easier by computing the average dynamics (averaged over one full period). Naive applications of this concept can lead to erroneous results, but there exists a rigorous theory of averaging; [20] provides an in-depth presentation of the topic. A key result used in this paper is the following: take a Π-periodic smooth dynamical system in the averaging canonical form:

$$\dot{\mathbf{x}} = \epsilon \boldsymbol{\phi}(\mathbf{x}, t, \epsilon) \tag{6}$$

with $\boldsymbol{\phi}$ Π-periodic and $0 < \epsilon << 1$ constant. The average dynamics are given by:

$$\bar{\boldsymbol{\phi}}(\mathbf{x}) = \frac{\epsilon}{\Pi} \int_0^{\Pi} \boldsymbol{\phi}(\mathbf{x}, t) dt \tag{7}$$

There are some theoretical bounds on the error of approximating $\boldsymbol{\phi}$ with $\bar{\boldsymbol{\phi}}$; however, a key limitation of the theory is that they only hold for a sufficiently small ϵ, without providing an explicit value thereof.

1.4.2 Floquet approach

Floquet theory allows for a rigorous analysis of the stability of time-periodic systems. While originally developed for linear systems, the approach can be generalized to nonlinear systems by linearizing them around a periodic orbit; the following brief outline of stability analysis provides an intuition for this particular case (for a rigorous introduction, see [19, 21]). Take a general periodic nonlinear system:

$$\dot{\mathbf{x}} = \boldsymbol{\phi}(\mathbf{x}, t) \tag{8}$$

Where $\boldsymbol{\phi}(x, t)$ is smooth and Π-periodic. Let $\mathbf{x}_\Pi(t)$ be a periodic solution of (8) such that $\mathbf{x}_\Pi(t) = \mathbf{x}_\Pi(t+\Pi)$ for all t. To discuss trajectories close to the periodic orbit, it is useful to introduce the time-dependent coordinate change:

$$\Delta\mathbf{x}(t) = \mathbf{x}(t) - \mathbf{x}_\Pi(t) \tag{9}$$

In the new coordinates, $\Delta\mathbf{x}(t) \equiv 0$ indicates a trajectory strictly following $\mathbf{x}_\Pi$. Intuitively, the periodic orbit can be considered stable if for any sufficiently small initial condition $\Delta\mathbf{x}(0) \neq 0$, the solution converges to 0 as $t \to \infty$ (i.e. when the trajectory converges to the periodic orbit). This notion is a key element of the Floquet analysis presented below.

Let $\Delta\mathbf{x}^{(i)}(t)$ be the response of system (8) to an initial condition $\Delta\mathbf{x}^{(i)}(0) = \epsilon\mathbf{e}_i$. This corresponds effectively to a small deviation from the periodic orbit in one of the state coordinates. The solution after one period Π is some value $\Delta\mathbf{x}^{(i)}(\Pi)$, which can be obtained by integrating (8) directly. Note that if ϵ is considered to be sufficiently small, the dynamics of $\Delta\mathbf{x}(t)$ can be considered to be linear (even if the periodic orbit as such is a result of nonlinear dynamics), meaning that $\Delta\mathbf{x}^{(i)}(\Pi)$ should be proportional to ϵ. Under this assumption, the dynamics of $\Delta\mathbf{x}$ over one period can be treated as a discrete linear time-invariant system given as follows:

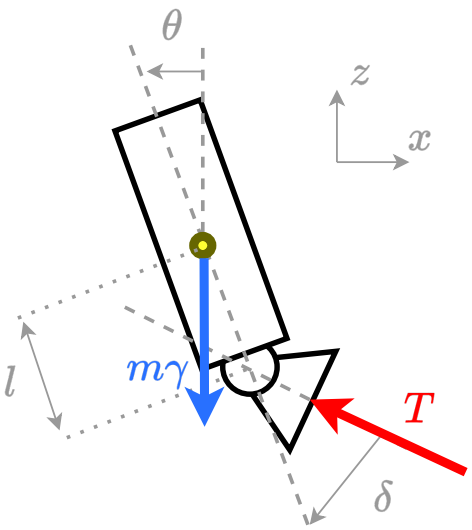

Fig. 1 Conceptual drawing of the system with key geometrical parameters.

$$\Delta\mathbf{x}(\Pi) = \boldsymbol{\mathcal{M}}\Delta\mathbf{x}(0) \tag{10}$$

Where $\boldsymbol{\mathcal{M}}$ is called the monodromy matrix of the system, and can be expressed as:

$$\boldsymbol{\mathcal{M}} = \frac{1}{\epsilon}\left[\Delta\mathbf{x}^{(1)}(\Pi) \quad \dots \quad \Delta\mathbf{x}^{(n)}(\Pi)\right] \tag{11}$$

When all of the eigenvalues of $\boldsymbol{\mathcal{M}}$ have a magnitude less than one, the periodic orbit $\mathbf{x}_\Pi(t)$ is stable. Note that this result is analogous to the stability analysis of a discrete linear time-invariant system, but under some mild assumptions it holds rigorously for the full continuous nonlinear system.

2 Analytical system analysis & control architecture

2.1 System

The rocket is modeled as a 2D rigid body under uniform gravitational acceleration γ and a thrust force T acting at angle δ with a lever arm l with respect to the center of gravity (see Figure 1 for reference):

$$\dot{\mathbf{x}} = \frac{d}{dt}\begin{bmatrix} p_x \\ p_z \\ v_x \\ v_z \\ \theta \\ q \end{bmatrix} = \begin{bmatrix} v_x \\ v_z \\ \frac{T}{m}\sin(\delta-\theta) \\ \frac{T}{m}\cos(\delta-\theta)-\gamma \\ q \\ \frac{Tl}{J}\sin\delta \end{bmatrix} = \begin{bmatrix} v_x \\ v_z \\ \frac{T}{m}(\sin\delta\cos\theta-\cos\delta\sin\theta) \\ \frac{T}{m}(\cos\delta\cos\theta+\sin\delta\sin\theta)-\gamma \\ q \\ \frac{Tl}{J}\sin\delta \end{bmatrix} = \boldsymbol{\phi}(\mathbf{x},\delta) \tag{12}$$

It is assumed that the angle δ is controlled directly, therefore ignoring the internal dynamics of the TVC system (however, the case study in section 3 presents a scenario where second order actuator dynamics are present). The thrust is assumed to be set at a constant value slightly greater than the weight $m\gamma$ (i.e. a thrust-to-weight ratio higher than 1), since it is trivial that a deficit of thrust cannot be compensated by

any control mechanism using δ alone, although in the more general reusable launcher case it could be partially compensated by drag-increasing devices such as airbrakes.

2.2 Controllability

For practical reasons, the controllability analysis is performed on a slightly different formulation of the system. First, since the positions p_x and p_z are the integrals of the respective velocities v_x and v_z, their controllability follows from the controllability of the velocities and they can be removed from the state vector without influencing the results (thus making the system smaller and easier to analyze). Then, since Lie bracket analysis requires a system in control-affine form (3), which (12) does not respect, δ is appended to the state, with its derivative $\dot{\delta}$ becoming the new input. The new state vector is therefore:

$$\tilde{\mathbf{x}} = \left[v_x, v_z, \theta, q, \delta\right]^T \tag{13}$$

The system dynamics can be now rewritten in terms of $\tilde{\mathbf{x}}$ and $\dot{\delta}$:

$$\dot{\tilde{\mathbf{x}}} = \begin{bmatrix} \boldsymbol{\phi}_{(3:6)}(\mathbf{x}, \delta) \\ 0 \end{bmatrix} + \begin{bmatrix} 0 \\ 1 \end{bmatrix} \dot{\delta} = \tilde{\mathbf{f}}(\tilde{\mathbf{x}}) + \tilde{\mathbf{g}}_{\dot{\delta}}(\tilde{\mathbf{x}})\dot{\delta} = \tilde{\boldsymbol{\phi}}(\tilde{\mathbf{x}}, \dot{\delta}) \tag{14}$$

where $\mathbf{x} = [0, 0, v_x, v_z, \theta, q]$ and $\boldsymbol{\phi}_{(3:6)}(\mathbf{x}, \delta)$ is $\boldsymbol{\phi}(\mathbf{x}, \delta)$ with the first two rows, corresponding to $\dot{p}_x$ and $\dot{p}_z$, omitted; the system is now in control-affine form and ready for Lie bracket analysis.

2.2.1 Linear

For the classical linear controllability analysis, the system must be first linearized:

$$\frac{\partial \tilde{\mathbf{f}}}{\partial \tilde{\mathbf{x}}}(\tilde{\mathbf{x}}, 0) = \tilde{\mathbf{A}}(\tilde{\mathbf{x}}) = \begin{bmatrix} 0 & 0 & -\frac{T}{m}\cos(\delta - \theta) & 0 & \frac{T}{m}\cos(\delta - \theta) \\ 0 & 0 & \frac{T}{m}\sin(\delta - \theta) & 0 & -\frac{T}{m}\sin(\delta - \theta) \\ 0 & 0 & 0 & 1 & 0 \\ 0 & 0 & 0 & 0 & \frac{Tl}{J}\cos\delta \\ 0 & 0 & 0 & 0 & 0 \end{bmatrix} \tag{15}$$

$$\frac{\partial \tilde{\mathbf{g}}_{\dot{\delta}}}{\partial \tilde{\mathbf{x}}}(\tilde{\mathbf{x}}, 0) = \tilde{\mathbf{B}}_{\dot{\delta}}(\tilde{\mathbf{x}}) = \begin{bmatrix} 0 & 0 & 0 & 0 & 1 \end{bmatrix}^T \tag{16}$$

The Kalman controllability matrix is then computed to be:

$$\boldsymbol{C}\left(\tilde{\mathbf{A}}(\tilde{\mathbf{x}}), \tilde{\mathbf{B}}_{\dot{\delta}}(\tilde{\mathbf{x}})\right) = \begin{bmatrix} 0 & \frac{T}{m}\cos(\theta - \delta) & 0 & -\frac{T^2 l}{Jm}\cos(\theta - \delta)\cos\delta & 0 \\ 0 & \frac{T}{m}\sin(\theta - \delta) & 0 & -\frac{T^2 l}{Jm}\sin(\theta - \delta)\cos\delta & 0 \\ 0 & 0 & \frac{Tl}{J}\cos\delta & 0 & 0 \\ 0 & \frac{Tl}{J}\cos\delta & 0 & 0 & 0 \\ 1 & 0 & 0 & 0 & 0 \end{bmatrix} \tag{17}$$

The system is clearly uncontrollable; not only is the row corresponding to v_z equal to 0 at $\tilde{\mathbf{x}} = \mathbf{0}$, but it is also linearly dependent on the first row at any $\tilde{\mathbf{x}} \neq \mathbf{0}$, seemingly confirming the conclusions from [7] that while the vertical movement can be controlled by exploiting the nonlinearities, there is a direct tradeoff in the horizontal controllability:

$$\boldsymbol{C}(\tilde{\mathbf{A}}\left(\tilde{\mathbf{x}}\right), \tilde{\mathbf{B}}_{\dot{\delta}}(\tilde{\mathbf{x}})) = \begin{bmatrix} 0 & \star & 0 & \star & 0 \\ 0 & \dagger & 0 & \dagger & 0 \\ 0 & 0 & \star & 0 & 0 \\ 0 & \star & 0 & 0 & 0 \\ \star & 0 & 0 & 0 & 0 \end{bmatrix} \begin{pmatrix} v_x \\ v_z \\ \theta \\ q \\ \delta \end{pmatrix} \tag{18}$$

2.2.2 Nonlinear

The computation of nested brackets of $\tilde{\mathbf{f}}$ and $\tilde{\mathbf{g}}_{\dot{\delta}}$ results in the following linearly independent terms (note that this solution is not unique, but it was chosen to be as simple as possible in terms of the maximum order of the brackets used):

$$\begin{aligned} \mathcal{L}\left(\tilde{\mathbf{f}}, \tilde{\mathbf{g}}_{\dot{\delta}}\right) &= \left[\tilde{\mathbf{g}}_{\dot{\delta}} \quad [\tilde{\mathbf{f}}, \tilde{\mathbf{g}}_{\dot{\delta}}] \quad [\tilde{\mathbf{f}}, [\tilde{\mathbf{f}}, \tilde{\mathbf{g}}_{\dot{\delta}}]] \quad [\tilde{\mathbf{f}}, [\tilde{\mathbf{f}}, [\tilde{\mathbf{f}}, \tilde{\mathbf{g}}_{\dot{\delta}}]]] \quad [[\tilde{\mathbf{f}}, \tilde{\mathbf{g}}_{\dot{\delta}}], \tilde{\mathbf{g}}_{\dot{\delta}}]\right] = \\ &= \begin{bmatrix} 0 & -\frac{T}{m}\cos(\theta-\delta) & \frac{T}{m}q\sin(\theta-\delta) & \frac{T}{Jm}\left(Jq^2\cos(\theta-\delta)+Tl\cos(\theta-2\delta)\right) & \frac{T}{m}\sin(\theta-\delta) \\ 0 & -\frac{T}{m}\sin(\theta-\delta) & -\frac{T}{m}q\cos(\theta-\delta) & \frac{T}{Jm}(Jq^2\sin(\theta-\delta)+Tl\sin(\theta-2\delta)) & -\frac{T}{m}\cos(\theta-\delta) \\ 0 & 0 & \frac{Tl}{J}\cos\delta & 0 & 0 \\ 0 & -\frac{Tl}{J}\cos\delta & 0 & 0 & -\frac{Tl}{J}\sin\delta \\ 1 & 0 & 0 & 0 & 0 \end{bmatrix} \end{aligned} \tag{19}$$

The resulting matrix is full rank even at $\tilde{\mathbf{x}} = 0$, which is a result strictly stronger than the local x-z controllability tradeoff observed in (18). Note that the matrices in (18) and (20) have similar structure, the only significant difference being the last column, corresponding to the Lie bracket $[[\tilde{\mathbf{f}}, \tilde{\mathbf{g}}_{\dot{\delta}}], \tilde{\mathbf{g}}_{\dot{\delta}}]$, which turns out to enable movement along the v_z direction (with smaller components in v_x and q, which can be compensated for, since the system is fully controllable).

$$\mathcal{L}\left(\tilde{\mathbf{f}}, \tilde{\mathbf{g}}_{\dot{\delta}}\right) = \begin{bmatrix} 0 & \star & \dagger & \star & \dagger \\ 0 & \dagger & \dagger & \dagger & \star \\ 0 & 0 & \star & 0 & 0 \\ 0 & \star & 0 & 0 & \dagger \\ \star & 0 & 0 & 0 & 0 \end{bmatrix} \begin{pmatrix} v_x \\ v_z \\ \theta \\ q \\ \delta \end{pmatrix} \tag{20}$$

2.3 Oscillatory thrust control

2.3.1 Intuition

The implementation of z axis control stems from a simple intuition: if the δ were to be periodically oscillated, the mean thrust experienced by the rocket would be reduced, with the lateral component canceling out over one full period. Assume that this oscillatory movement is sinusoidal:

$$\delta_{\text{osc}}(t) = \Delta\sin(\omega t) \tag{21}$$

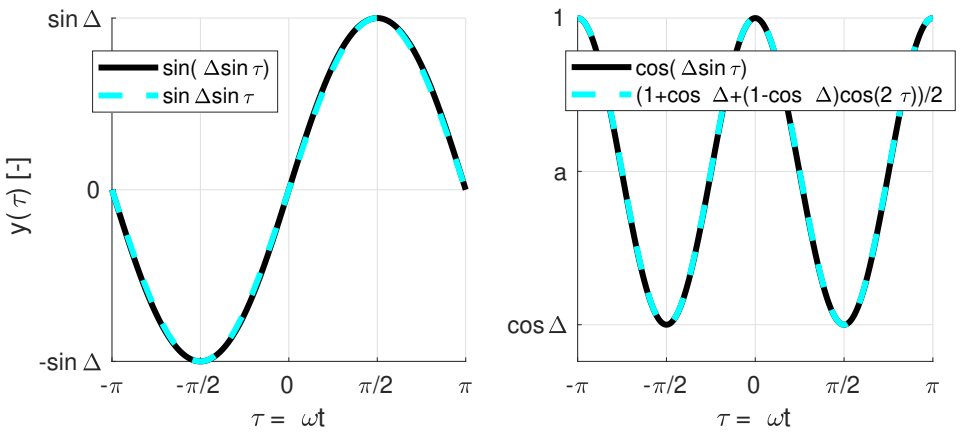

Fig. 2 Trigonometric approximations found in (23) **and** (24) **compared with exact values for** $\Delta = \delta_{\max} = 30°$**.**

First, a simplified analysis is performed by neglecting any induced pitching movement; the mean axial component of thrust resulting from such oscillations can be computed as:

$$\bar{T} = \frac{1}{\Pi}\int_0^{\Pi} T\cos\left(\Delta\sin(\omega t)\right)\mathrm{d}t \tag{22}$$

Where $\Pi = 2\pi/\omega$ is the period of oscillation. The integral in (22) is not trivial, but for moderate Δ it can be simplified using the following approximation:

$$\cos(\Delta\sin(\omega t)) \approx \frac{1+\cos\Delta}{2} + \frac{1-\cos\Delta}{2}\cos(2\omega t) = a(\Delta) + b(\Delta)\cos(2\omega t) \tag{23}$$

where the Δ-dependency of constants a and b will be omitted in the rest of the paper to simplify notation. The right part of Figure 2 presents the high accuracy of this approximation for $\Delta = 30°$, which is the maximal Δ considered in this paper (since $\delta_{\max} = 30°$ is assumed in section 3).

While the average thrust in the perpendicular direction is trivially zero, a trigonometric approximation analogous to (23), which could allow to compute it, will be useful for later computations:

$$\sin\left(\Delta\sin(\omega t)\right) \approx \sin\Delta\sin(\omega t) = c(\Delta)\sin(\omega t) \tag{24}$$

The accuracy of this approximation can be seen in the left part of Figure 2. The Δ-dependency of c will also be omitted in notation from now on. Substituting (23) back into (22), the mean z-axis thrust can be computed:

$$\bar{T} \approx \frac{T}{\Pi}\int_0^{\Pi}\left(a + b\cos(2\omega t)\right)\mathrm{d}t = \frac{T}{\Pi}\left(\int_0^{\Pi} a\mathrm{d}t + \frac{b}{\omega}\int_0^{2\pi}\cos\tau\mathrm{d}\tau\right) = Ta = T\frac{1+\cos\Delta}{2} \tag{25}$$

This mean value behaves as expected, with $\bar{T} = T$ for $\Delta = 0$ and gradually decreasing for higher Δ, and remains consistent with the exact values of $\bar{T}$ given by (22) (see Figure 3), with a relative error under 1% for all feasible TVC angles (see Figure 4).

To obtain a certain difference ΔT in effective thrust, the necessary Δ is:

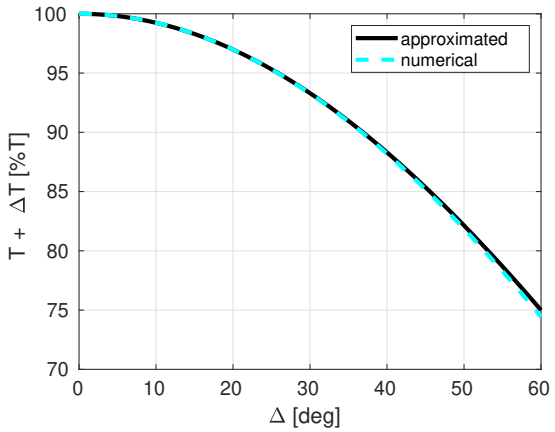

Fig. 3 Minimum obtainable values of average thrust $\bar{T}$ as a function of the TVC oscillation amplitude Δ. The approximated value is computed using (25), while the numerical value is the result of applying first order numerical integration to solve (22).

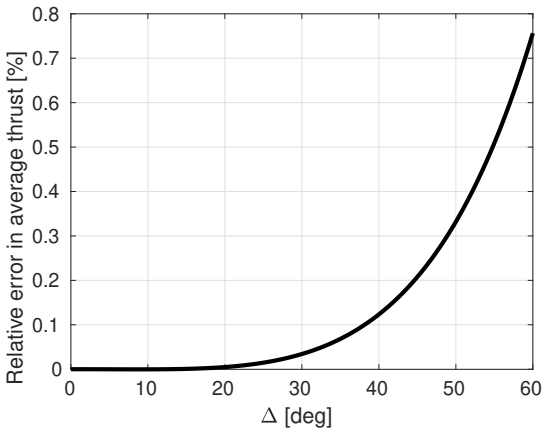

Fig. 4 Relative error of $\bar{T}$ due to using the approximate analytical expression (25) instead of the full integral (22) (as shown in Figure 3).

$$\bar{T} = T + \Delta T = T\frac{1+\cos\Delta}{2} \Rightarrow \Delta = \arccos\left(2\frac{\Delta T}{T} + 1\right) \tag{26}$$

Note that Δ exists only for non-positive ΔT, confirming our intuition that the oscillation mechanism can only reduce thrust, not increase it. The upper bound for ΔT is therefore $\Delta T_{\max} = 0$, while the lower bound depends on the maximal value of Δ attainable by the system:

$$\Delta T_{\min} = T\frac{\cos\Delta_{\max} - 1}{2} \tag{27}$$

Since a simple controlled landing requires the rocket to be able to descend in a controlled manner, the average thrust must be possible to be made lower than the weight $m\gamma$ (note that for a well planned landing trajectory this is not necessary, since the rocket can be decelerating for the entirety of its landing sequence; the result in (27) is more fundamental than the following bounds):

$$\bar{T} = T + \Delta T < m\gamma \Rightarrow \Delta T \leq m\gamma - T \tag{28}$$

Combining with (27), this gives the following upper bound on the thrust-to-weight ratio that can be compensated by the oscillatory mechanism:

$$\left(\frac{T}{m\gamma}\right)_{\max} = \frac{2}{1+\cos\Delta_{\max}} = \frac{1}{a_{\min}} \tag{29}$$

For the value of $\Delta_{\max} = 30°$ considered in this paper, this gives a maximum compensable thrust-to-weight ratio of around 1.072. The inverse of this value, 0.933, is the minimum attainable value of the thrust reduction factor a.

(26) implies that oscillatory control, as given by (21), can indirectly control the mean thrust $\bar{T}$; furthermore, since $\bar{\delta}_{\text{osc}} = 0$, it still seems to be possible to actuate the system using mean δ independently of the thrust control, with the limitation that the bandwidth of such additional actuation should be inferior to ω. The following sections will rigorously show that this is indeed possible.

2.3.2 Average dynamics

The calculations in the previous subsection made the assumption that the rocket performs no significant movement during the oscillation cycle. To verify whether the expected thrust reduction actually occurs in the full dynamical system, averaging theory can be used. The system will be assumed to be actuated by the input:

$$\delta(t) = \Delta \sin(\omega t) + \bar{\delta}(t) = \delta_{\text{osc}}(t) + \bar{\delta}(t) \tag{30}$$

where $\bar{\delta}(t)$ is an arbitrary control signal acting on top of the oscillatory control, without explicit time dependency; it is denoted as a mean since the oscillatory part has zero mean, meaning that the mean of δ is just the mean of $\bar{\delta}$. The time dependence of the components of $\delta(t)$ will be omitted to shorten the notation. The system dynamics, as shown in (12), actuated by (30) are:

$$\begin{aligned}
\frac{d}{dt}\begin{bmatrix} p_x \\ p_z \\ v_x \\ v_z \\ \theta \\ q \end{bmatrix} &= \begin{bmatrix} v_x \\ v_z \\ \frac{T}{m}\left(\sin(\delta_{\text{osc}}+\bar{\delta})\cos\theta - \cos(\delta_{\text{osc}}+\bar{\delta})\sin\theta\right) \\ \frac{T}{m}\left(\cos(\delta_{\text{osc}}+\bar{\delta})\cos\theta + \sin(\delta_{\text{osc}}+\bar{\delta})\sin\theta\right) - \gamma \\ q \\ \frac{Tl}{J}\sin(\delta_{\text{osc}}+\bar{\delta}) \end{bmatrix} = \\
&= \begin{bmatrix} v_x \\ v_z \\ \frac{T}{m}\left(\cos\delta_{\text{osc}}\sin(\bar{\delta}-\theta) + \sin\delta_{\text{osc}}\cos(\bar{\delta}-\theta)\right) \\ \frac{T}{m}\left(\cos\delta_{\text{osc}}\cos(\bar{\delta}-\theta) - \sin\delta_{\text{osc}}\sin(\bar{\delta}-\theta)\right) - \gamma \\ q \\ \frac{Tl}{J}\left(\cos\delta_{\text{osc}}\sin\bar{\delta} + \sin\delta_{\text{osc}}\cos\bar{\delta}\right) \end{bmatrix} = \\
&= \begin{bmatrix} v_x \\ v_z \\ \frac{T}{m}\left((a+b\cos(2\omega t))\sin(\bar{\delta}-\theta) + c\sin(\omega t)\cos(\bar{\delta}-\theta)\right) \\ \frac{T}{m}\left((a+b\cos(2\omega t))\cos(\bar{\delta}-\theta) - c\sin(\omega t)\sin(\bar{\delta}-\theta)\right) - \gamma \\ q \\ \frac{Tl}{J}\left((a+b\cos(2\omega t))\sin\bar{\delta} + c\sin(\omega t)\cos\bar{\delta}\right) \end{bmatrix}
\end{aligned} \tag{31}$$

To apply averaging, the system needs to be in the standard form (6). While the system in (31) is not in this form, it can be easily transformed by introducing a new time variable in the time scale of the δ oscillation:

$$\tau = \omega t \tag{32}$$

Substituting (32) to (31), and splitting the resulting expression into a time-dependent and time-independent part results in:

$$\mathbf{x}'(\tau) = \frac{d}{d\tau}\begin{bmatrix} p_x \\ p_z \\ v_x \\ v_z \\ \theta \\ q \end{bmatrix} = \frac{1}{\omega}\begin{bmatrix} v_x \\ v_z \\ \frac{T}{m} a \sin(\bar{\delta} - \theta) \\ \frac{T}{m} a \cos(\bar{\delta} - \theta) - \gamma \\ q \\ \frac{Tal}{J} \sin\bar{\delta} \end{bmatrix} + \frac{1}{\omega}\begin{bmatrix} 0 \\ 0 \\ \frac{T}{m}\left(b \sin(\bar{\delta} - \theta)\cos(2\tau) + c\cos(\bar{\delta} - \theta)\sin\tau\right) \\ \frac{T}{m}\left(b \cos(\bar{\delta} - \theta)\cos(2\tau) - c\sin(\bar{\delta} - \theta)\sin\tau\right) \\ 0 \\ \frac{Tl}{J}\left(b \sin\bar{\delta}\cos(2\tau) + c\cos\bar{\delta}\sin\tau\right) \end{bmatrix} = \tag{33}$$
$$= \frac{1}{\omega}\left(\mathbf{r}_{\text{osc}}(\mathbf{x}) + \mathbf{s}_{\text{osc}}(\mathbf{x}, \tau)\right) = \frac{1}{\omega}\boldsymbol{\phi}_{\text{osc}}(\mathbf{x}, \tau)$$

In the expression above, $1/\omega$ satisfies the role of ϵ in (6). This is all the more justified because $1/\omega$ can indeed be made arbitrarily small by increasing the oscillation frequency correspondingly. The average is easily computed since s_{osc} has 0 mean over one time period:

$$\bar{\mathbf{x}}' = \frac{1}{\omega}\left(\bar{r}_{\text{osc}}(\bar{\mathbf{x}}) + \bar{\mathbf{s}}_{\text{osc}}(\bar{\mathbf{x}}, \tau)\right) = \frac{1}{w\Pi}\int_0^{\Pi} \mathbf{r}_{\text{osc}}(\mathbf{x})\mathrm{d}\tau = \frac{1}{\omega} f(\bar{\mathbf{x}}) \tag{34}$$

Converting back to standard time, the average dynamics are:

$$\dot{\bar{\mathbf{x}}} = \frac{d}{dt}\begin{bmatrix} \bar{p}_x \\ \bar{p}_z \\ \bar{v}_x \\ \bar{v}_z \\ \bar{\theta} \\ \bar{q} \end{bmatrix} = \begin{bmatrix} \bar{v}_x \\ \bar{v}_z \\ \frac{T}{m} a \sin(\bar{\delta} - \bar{\theta}) \\ \frac{T}{m} a \cos(\bar{\delta} - \bar{\theta}) - \gamma \\ \bar{q} \\ \frac{Tal}{J} \sin\bar{\delta} \end{bmatrix} = \begin{bmatrix} \bar{v}_x \\ \bar{v}_z \\ (T + \Delta T)\frac{1}{m} \sin(\bar{\delta} - \bar{\theta}) \\ (T + \Delta T)\frac{1}{m} \cos(\bar{\delta} - \bar{\theta}) - \gamma \\ \bar{q} \\ (T + \Delta T)\frac{l}{J} \sin\bar{\delta} \end{bmatrix} = \bar{\boldsymbol{\phi}}(\bar{\mathbf{x}}, \bar{u}) \tag{35}$$

with $\bar{u} = [\bar{\delta}, \Delta T]^T$. The average dynamics under oscillatory control are therefore exactly the original dynamics (12) with δ replaced by $\bar{\delta}$ (which can still be arbitrary, as long as no explicit time dependence is involved) and with the original thrust multiplied by the factor a, just as predicted in (25); for convenience, the mean thrust Ta will be written as the sum of the raw value and mean increment, $T + \Delta T$. ΔT can be indirectly controlled by modulating Δ, while retaining independent control of $\bar{\delta}$. This means that the averaged system has two independent inputs: $\bar{\delta}$ and the thrust increment ΔT, in practice modulated by Δ.

2.3.3 Controllability

It can be shown that the average system (35) is fully controllable even in the linear sense. To save space and maintain consistency with the previous results in (18) and (20), the input will be defined as:

$$\bar{u} = \begin{bmatrix} \dot{\bar{\delta}} \\ \Delta T \end{bmatrix} \tag{36}$$

while the state will be:

$$\bar{\bar{\mathbf{x}}} = \begin{bmatrix} \bar{v}_x & \bar{v}_z & \bar{\theta} & \bar{q} & \bar{\delta} \end{bmatrix}^T \tag{37}$$

The linearized state transition matrix is:

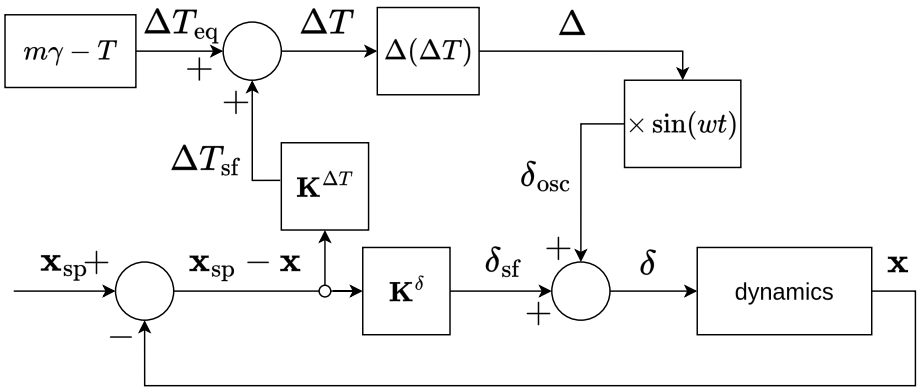

Fig. 5 Block diagram of proposed control architecture.

$$\bar{\bar{\mathbf{A}}}(\bar{\bar{\mathbf{x}}}) = \frac{\partial \bar{\boldsymbol{\phi}}}{\partial \bar{\bar{\mathbf{x}}}} = \begin{bmatrix} 0 & 0 & -\frac{T}{m}\cos(\bar{\delta}-\bar{\theta}) & 0 & \frac{T}{m}\cos(\bar{\delta}-\bar{\theta}) \\ 0 & 0 & \frac{T}{m}\sin(\bar{\delta}-\bar{\theta}) & 0 & = \frac{T}{m}\sin(\bar{\delta}-\bar{\theta}) \\ 0 & 0 & 0 & 1 & 0 \\ 0 & 0 & 0 & 0 & \frac{Tl}{J}\cos\bar{\delta} \\ 0 & 0 & 0 & 0 & 0 \end{bmatrix} \tag{38}$$

The input matrix corresponding to $\bar{u}$ is:

$$\bar{\bar{\mathbf{B}}}(\bar{\bar{\mathbf{x}}}) = \frac{\partial \bar{\boldsymbol{\phi}}}{\partial \bar{u}} = \begin{bmatrix} 0 & \frac{1}{m}\sin(\bar{\delta}-\bar{\theta}) \\ 0 & \frac{1}{m}\cos(\bar{\delta}-\bar{\theta}) \\ 0 & 0 \\ 0 & \frac{l}{J}\sin\bar{\delta} \\ 1 & 0 \end{bmatrix} \tag{39}$$

The Kalman controllability matrix, evaluated at the equilibrium point corresponding to hover, defined by $\bar{\bar{\mathbf{x}}}_{\text{eq}} = [0,0,0,0,0]^T$ and $\bar{u}_{\text{eq}} = [0, m\gamma - T]^T$, is (only the shorthand notation is shown, since the full symbolic expression is too long to fit on a page):

$$\boldsymbol{C}\left(\bar{\bar{\mathbf{A}}}(\bar{\bar{\mathbf{x}}}_{\text{eq}}), \bar{\bar{\mathbf{B}}}(\bar{\bar{\mathbf{x}}}_{\text{eq}})\right) = \begin{bmatrix} 0 & \dagger & \star & 0 & 0 & \dagger & \star & 0 & \cdots & 0 \\ 0 & \star & \dagger & 0 & 0 & \dagger & \dagger & 0 & & 0 \\ 0 & 0 & 0 & \dagger & \star & 0 & 0 & 0 & \ddots & 0 \\ 0 & \dagger & \star & 0 & 0 & 0 & 0 & 0 & & 0 \\ \star & 0 & 0 & 0 & 0 & 0 & 0 & 0 & \cdots & 0 \end{bmatrix} \begin{pmatrix} \bar{v}_x \\ \bar{v}_z \\ \bar{\theta} \\ \bar{q} \\ \bar{\delta} \end{pmatrix} \tag{40}$$

The Kalman matrix is full rank even exactly at the equilibrium point, meaning that the system is indeed full controllable (at least locally).

2.4 Stabilizing controller

The average system, as given by (35), is not fully stable (see subsubsection 3.1.2 for more details), but since it is controllable, it can be stabilized using feedback control; the same is expected from the full system (12). To achieve stability in the vertical axis, it is necessary to control the virtual input ΔT. The proposed control law is a simple proportional state feedback:

$$\Delta T_{\text{sf}} = \mathbf{K}^{\Delta T}(\mathbf{x}_{\text{sp}} - \mathbf{x}) = \begin{bmatrix} K_{p_x}^{\Delta T} & K_{p_z}^{\Delta T} & K_{v_x}^{\Delta T} & K_{v_z}^{\Delta T} & K_{\theta}^{\Delta T} & K_{q}^{\Delta T} \end{bmatrix} (\mathbf{x}_{\text{sp}} - \mathbf{x}) \tag{41}$$

where $\mathbf{x}_{\text{sp}}$ is the state setpoint. Moreover, since stationary hover is the flight condition used for analysis, it is useful to add a feedforward term that will keep the rocket stationary in hover by reducing the mean thrust to exactly compensate for the weight $m\gamma$:

$$\Delta T_{\text{eq}} = m\gamma - T \tag{42}$$

The resulting control law on ΔT is:

$$\Delta T_{\text{cl}} = \Delta T_{\text{eq}} + \Delta T_{\text{sf}} = m\gamma - T + \mathbf{K}^{\Delta T}(\mathbf{x}_{\text{sp}} - \mathbf{x}) \tag{43}$$

ΔT is not, however, controlled directly; it is modulated using Δ as given by (26). Combining the two equations results in the following control law:

$$\begin{aligned} \Delta(\mathbf{x}) &= \arccos\left(1 + \frac{2}{T}(m\gamma - T + \mathbf{K}^{\Delta T}(\mathbf{x}_{\text{sp}} - \mathbf{x}))\right) \\ &= \arccos\left(-1 + \frac{2}{T}(m\gamma + \mathbf{K}^{\Delta T}(\mathbf{x}_{\text{sp}} - \mathbf{x}))\right) \end{aligned} \tag{44}$$

For δ, a simple linear state feedback law is proposed:

$$\delta_{\text{sf}}(\mathbf{x}, t) = \mathbf{K}^{\delta}(\mathbf{x}_{\text{sp}} - \mathbf{x}) = \begin{bmatrix} K_{p_x}^{\delta} & K_{p_z}^{\delta} & K_{v_x}^{\delta} & K_{v_z}^{\delta} & K_{\theta}^{\delta} & K_{q}^{\delta} \end{bmatrix} (\mathbf{x}_{\text{sp}} - \mathbf{x}) \tag{45}$$

This control law is combined with the oscillatory control given by (21), resulting in the following control law on δ:

$$\delta_{\text{cl}}(\mathbf{x}, t) = \delta_{\text{osc}}(t) + \delta_{\text{sf}}(t) = \Delta(\mathbf{x}) \sin(\omega t) + \mathbf{K}^{\delta}(\mathbf{x}_{\text{sp}} - \mathbf{x}) \tag{46}$$

The resulting control architecture is shown in Figure 5.

2.5 Averaged closed-loop dynamics

To obtain the averaged closed-loop dynamics, an analysis such as the one in subsubsection 2.3.2 should be performed. However, in this specific case, the result is equivalent to performing two rather intuitive substitutions in the original result in (35). Assuming that the value of ΔT_{cl} remains in the interval $[\Delta T_{\min}, 1]$, as defined by (27), (43) can be substituted directly into the mean dynamics in (35), which simplifies the analysis. Therefore, since the effect of δ_{osc} is already taken into account, the only component of δ_{cl} left is δ_{sf}, which can be directly substituted in of $\bar{\delta}$ in (35), since it is not explicitly time-dependent. This results in the following closed-loop dynamics:

$$\dot{\bar{\mathbf{x}}} = \frac{d}{dt}\begin{bmatrix}\bar{p}_x\\ \bar{p}_z\\ \bar{v}_x\\ \bar{v}_z\\ \bar{\theta}\\ \bar{q}\end{bmatrix} = \begin{bmatrix}\bar{v}_x\\ \bar{v}_z\\ (\gamma + \frac{1}{m}K^{\Delta T}(\mathbf{x}_{\text{sp}} - \bar{\mathbf{x}}))\sin(K^{\delta}(\mathbf{x}_{\text{sp}} - \bar{\mathbf{x}}) - \bar{\theta})\\ (\gamma + \frac{1}{m}K^{\Delta T}(\mathbf{x}_{\text{sp}} - \bar{\mathbf{x}}))\cos(K^{\delta}(\mathbf{x}_{\text{sp}} - \bar{\mathbf{x}}) - \bar{\theta}) - \gamma\\ \bar{q}\\ (m\gamma + K^{\Delta T}(\mathbf{x}_{\text{sp}} - \bar{\mathbf{x}}))\frac{l}{J}\sin(K^{\delta}(\mathbf{x}_{\text{sp}} - \bar{\mathbf{x}}))\end{bmatrix} = \bar{\boldsymbol{\phi}}_{\text{cl}}(\bar{\mathbf{x}}, \mathbf{x}_{\text{sp}}) \tag{47}$$

Assuming that the setpoint is $\mathbf{x}_{\text{sp}} = [0, 0, 0, 0, 0, 0]^T$, the equation above simplifies to:

$$\dot{\bar{\mathbf{x}}} = \frac{d}{dt}\begin{bmatrix}\bar{p}_x\\ \bar{p}_z\\ \bar{v}_x\\ \bar{v}_z\\ \bar{\theta}\\ \bar{q}\end{bmatrix} = \begin{bmatrix}\bar{v}_x\\ \bar{v}_z\\ (\frac{1}{m}\mathbf{K}^{\Delta T}\bar{\mathbf{x}} - \gamma)\sin(\mathbf{K}^{\delta}\bar{\mathbf{x}} + \bar{\theta})\\ (\gamma - \frac{1}{m}\mathbf{K}^{\Delta T}\bar{\mathbf{x}})\cos(\mathbf{K}^{\delta}\bar{\mathbf{x}} + \bar{\theta}) - \gamma\\ \bar{q}\\ (\mathbf{K}^{\Delta T}\bar{\mathbf{x}} - m\gamma)\frac{l}{J}\sin(\mathbf{K}^{\delta}\bar{\mathbf{x}})\end{bmatrix} = \bar{\boldsymbol{\phi}}_{\text{cl}}(\bar{\mathbf{x}}, \mathbf{x}_{\text{sp}}) \tag{48}$$

3 Numerical study

3.1 Setup

3.1.1 Open loop system

The values chosen for the physical parameters of the rocket are listed in Table 1; the CG position and inertial values were taken from [7] in order to enable a direct comparison of results with the article in question; note that it considers a model rocket, in hope of being able to experimentally test the proposed control scheme in the future.

Table 1 Physical parameters of the rocket (mass & geometry taken from [7]).

Symbol	Meaning	Value	Unit
$\delta_{\max}$	maximum TVC angle	±30	°
γ	gravitational acceleration	9.81	$\text{m} \cdot \text{s}^{-2}$
J	moment of inertia w.r.t. CG	0.12	$\text{kg} \cdot \text{m}^2$
l	lever arm of thrust w.r.t. CG	0.52	m
$\frac{T}{m\gamma}$	thrust-to-weight ratio	1.03	–
m	mass	3	kg

3.1.2 Feedback control

Since the feedback laws in (41) and (45) are effectively linear state feedback (with ΔT_{sf} being a virtual input to the system, as discussed in subsubsection 2.3.2), a simple pragmatic idea to tune the gains $\mathbf{K}^{\Delta T}$ and $\mathbf{K}^{\delta}$ is to use LQR synthesis on the linearized mean system (35). The point of analysis is chosen to be stationary hover at $\mathbf{x}_{\text{eq}} = [0, 0, 0, 0, 0, 0]^T$. The linearized system matrices are:

$$\bar{\mathbf{A}}_{\text{ol}} = \frac{\partial \bar{\boldsymbol{\phi}}}{\partial \bar{\mathbf{x}}}(\bar{\mathbf{x}}_{\text{eq}}, 0) = \begin{bmatrix} 0 & 0 & 1 & 0 & 0 & 0 \\ 0 & 0 & 0 & 1 & 0 & 0 \\ 0 & 0 & 0 & 0 & -\gamma & 0 \\ 0 & 0 & 0 & 0 & 0 & 0 \\ 0 & 0 & 0 & 0 & 0 & 1 \\ 0 & 0 & 0 & 0 & 0 & 0 \end{bmatrix} \tag{49}$$

$$\bar{\mathbf{B}}_{\text{ol}} = \begin{bmatrix} \frac{\partial \bar{\boldsymbol{\phi}}}{\partial \bar{\delta}}(\bar{\mathbf{x}}_{\text{eq}}, 0) \\ \frac{\partial \bar{\boldsymbol{\phi}}}{\partial \Delta T}(\bar{\mathbf{x}}_{\text{eq}}, 0) \end{bmatrix} = \begin{bmatrix} 0 & 0 \\ 0 & 0 \\ \gamma & 0 \\ 0 & \frac{1}{m} \\ 0 & 0 \\ \frac{\gamma l m}{J} & 0 \end{bmatrix} \tag{50}$$

Note that since $\bar{\mathbf{A}}_{\text{ol}}$ is an upper-triangular matrix with a zero diagonal, its eigenvalues must be 0, meaning that the linearized system is marginally stable. After some empirical tuning, the cost matrices were chosen to be as follows:

$$\mathbf{Q} = \text{diag}([1, 1, 1, 100, 1, 0.1]) \tag{51}$$

$$\mathbf{R} = \begin{bmatrix} 10 & 0 \\ 0 & 1 \end{bmatrix} \tag{52}$$

This results in the LQR feedback gains:

$$\mathbf{K} = \begin{bmatrix} \mathbf{K}^{\delta} \\ \mathbf{K}^{\Delta T} \end{bmatrix} \approx \begin{bmatrix} -0.32 & 0 & -0.43 & 0 & 1.3 & 0.21 \\ 0 & 1 & 0 & 10 & 0 & 0 \end{bmatrix} \tag{53}$$

The gain matrix has a very intuitive structure: $\mathbf{K}^{\delta}$ stabilizes the attitude and horizontal dynamics, while $\mathbf{K}^{\Delta T}$ stabilizes the vertical dynamics. The linearized state transition matrix of the closed-loop system is:

$$\bar{\mathbf{A}}_{\text{cl}} = \frac{\partial \bar{\boldsymbol{\phi}}}{\partial \bar{\mathbf{x}}}(\bar{\mathbf{x}}_{\text{eq}}) = \begin{bmatrix} 0 & 0 & 1 & 0 & 0 & 0 \\ 0 & 0 & 0 & 1 & 0 & 0 \\ -K^{\delta}_{p_x} & 0 & -K^{\delta}_{v_x} & 0 & -\gamma(K^{\delta}_{\theta} + 1) & -\gamma K^{\delta}_{q} \\ 0 & -K^{\Delta T}_{p_z} & 0 & -K^{\Delta T}_{p_z} & 0 & 0 \\ 0 & 0 & 0 & 0 & 0 & 1 \\ -K^{\delta}_{p_x}\mathcal{J} & 0 & -K^{\delta}_{v_x}\mathcal{J} & 0 & -K^{\delta}_{\theta}\mathcal{J} & -K^{\delta}_{q}\mathcal{J} \end{bmatrix} \tag{54}$$

Where $\mathcal{J} = \frac{\gamma^2 l m^2}{J T}$. After substituting in the numerical values of parameters from Table 1 and (53), the eigenvalues of $\bar{\mathbf{A}}_{\text{cl}}$ can be computed; the results are summarized in Table 2. Since all of the eigenvalues have a negative real part (with the smallest damping ratio being 0.81), the averaged dynamics are stable in hover in the analyzed case. Given the limitations of averaging theory, this result is only assured for sufficiently high values of ω. Naturally, the physical TVC system has a bandwidth imposed by the actuators used; rather than being arbitrarily high, ω is in practice limited to a few Hz at most. However,

the oscillatory control can be practically implemented with a small value of ω; a value of 3 Hz is used in the following sections as an example. First, the accuracy of averaged dynamics under low frequency is shown in subsection 3.2; then, the stability of the full nonlinear time-dependent system under feedback control is demonstrated using Floquet theory in subsection 3.3.

Table 2 Numerical values of eigenvalues of $\bar{\mathbf{A}}_{\text{cl}}$ (equation (54)).

Eigenvalue	Damping ratio [-]	Frequency [rad/s]	Key states
-1.00	1.00	1.00	p_x, v_x
-4.55 ± i3.35	0.81	5.65	ω, v_z, θ
-12.3	1.00	12.3	ω
-0.0981	1.00	0.0981	p_z
-10.2	1.00	10.2	v_z

3.2 Maneuver simulation

3.2.1 Scenario

The behavior of the proposed control architecture is demonstrated on a simple landing maneuver, with an initial state $\mathbf{x}(0) = [-2, 2, 0, 0, 0, 0]^T$ slightly above the ground and to the left of the desired landing spot $\mathbf{x}_{\text{sp}} = [0, 0, 0, -0.3, 0, 0]^T$ (where $(v_z)_{\text{sp}}$ is set to -0.3 since the landing speed does not need to be arbitrarily low) to demonstrate simultaneous lateral and vertical control. The ω value is chosen to be small (the current scenario corresponding to a frequency of $\nu = 3$ [Hz]), to emphasize that the oscillatory control is viable even though it was synthesized with the implicit assumption of high frequency. The equations of motion are integrated using a 4^{th} order Runge-Kutta scheme with a timestep of $\Pi/200 = 1.7 \cdot 10^{-3}$ [s]. As for the equations of motion, 3 scenarios are considered (each with the same control gains presented before):

1) **full dynamics** – closed-loop given by (12) with the control law defined in (46)
2) **averaged dynamics** – given by (47)
3) **full dynamics with actuator model** – the full dynamics augmented by a second order actuator model on the TVC angle δ with natural frequency $\omega_{\text{a}} = 50$ [rad/s] and damping $\zeta_{\text{a}} = 0.7$ – to demonstrate that the control law still works for an imperfect plant model.

3.2.2 Results

Figure 6 shows the evolution of $\mathbf{x}$ and $\bar{\mathbf{x}}$ in the landing maneuver scenario. Despite the low value of ω (equivalent to 3 Hz), the average states follow the full dynamics for the entire duration of the simulation. The oscillatory action has a very visible effect on q, with an amplitude in the order of 100-200 rad/s; however, this leads to pitch and velocity oscillations of only around 5 °/s and less than 0.1 $\frac{\text{m}}{\text{s}}$, respectively; in the position curves, the oscillations are virtually invisible.

The control inputs of this scenario are displayed in Figure 7. In the first plot, you can see that after the initial transient, $\delta(t)$ is dominated by oscillatory behavior related to δ_{osc}; however, there is a slight phase shift due to δ_{sf} reacting to the vehicle oscillations induced by δ_{osc}. In the third plot, it can be seen that this reaction is chiefly due to oscillations in ω, with smaller components from θ and v_x. The thrust increment $\Delta T(t)$ and its components is shown in the middle plot; the three components of the $\Delta T(t)$ are the constant ΔT_{eq}, the p_z term gradually increasing as the rocket gets closer to the ground, and the v_z term which first causes a downward overshoot and gradually recovers to land with a velocity very close to the specified value.

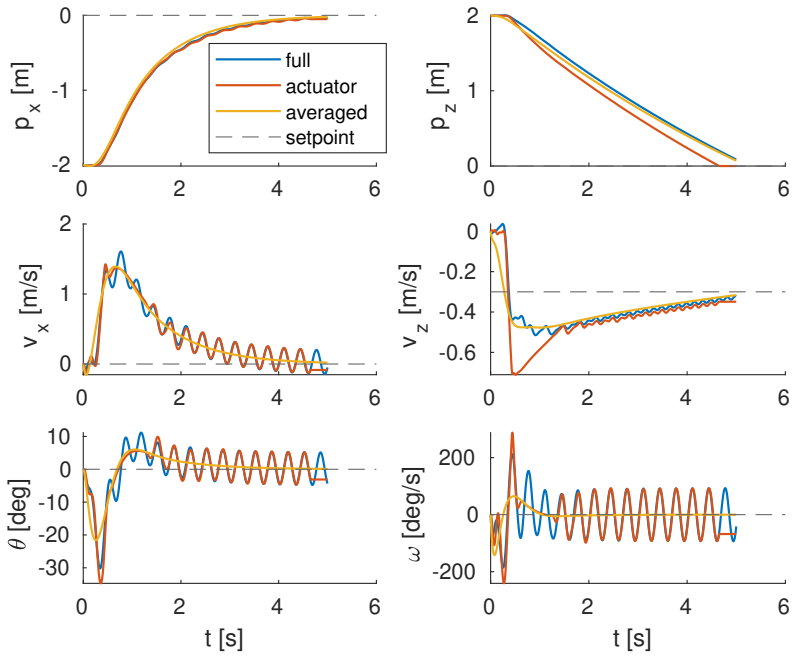

Fig. 6 State evolution in the landing maneuver simulation scenarios.

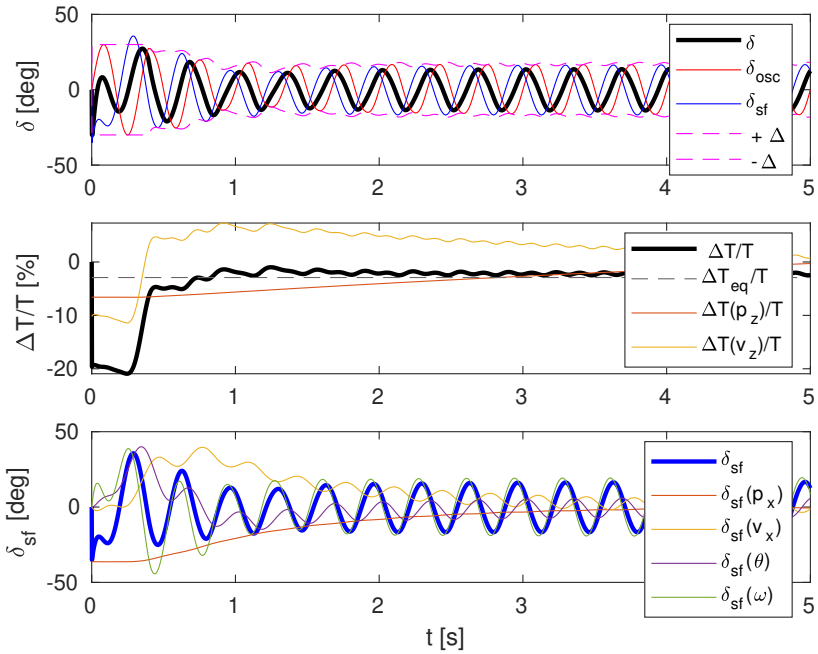

Fig. 7 Control inputs in the full dynamics variant of the landing maneuver simulation scenario.

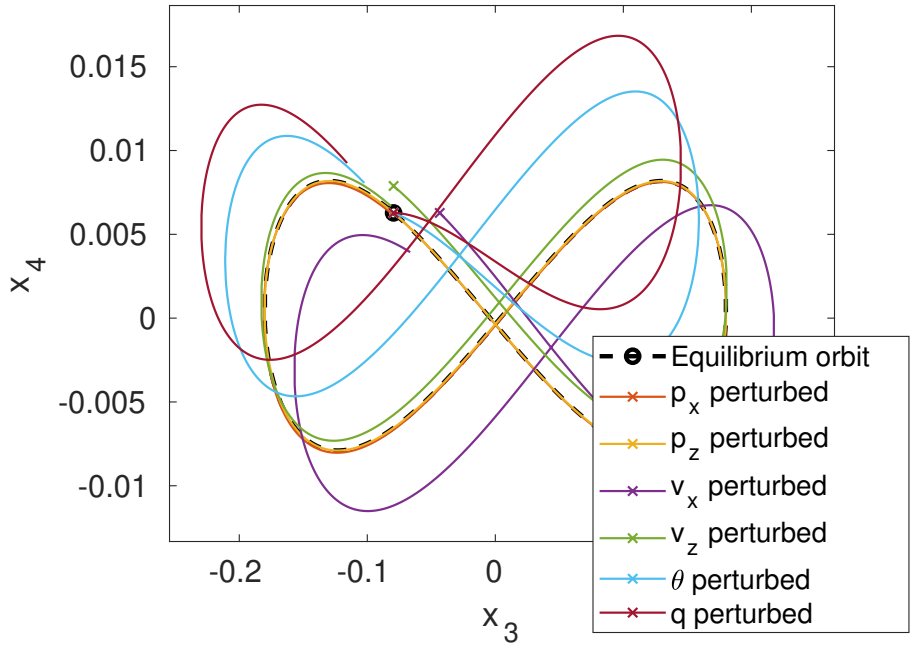

Fig. 8 v_x **and** v_z **coordinates of the periodic orbit** $\mathbf{x}_\Pi(t)$ **(dashed black) and perturbed orbits** $\mathbf{x}_\Pi^{(i)}(t)$**. The starting points are denoted by the o and x markers.**

As for the actuator scenario, in Figure 6 it can be seen that there is a rather good match with the nominal scenario, with the biggest difference being a larger dip in vertical velocity in the first 2 seconds of the maneuver. Overall, this demonstrates that the control scheme has a certain capacity for accommodating unmodeled dynamics. It is worth noting, however, that while in the nominal case the system was successfully stabilized using almost any oscillation frequency in the $\nu \in [0.4, 5]$ [Hz] range (as discussed later in subsection 3.3), with the actuator model in place finding suitable values of ν proved harder, with some values resulting in unstable or quasi-periodic behavior. This would suggest that in a practical application ν might need to be chosen using either experimental tests or high-fidelity simulation.

3.3 Floquet analysis

The stability of the rocket in hover can be shown using the Floquet approach, as outlined in subsubsection 1.4.2. A periodic orbit $\mathbf{x}_\Pi(t)$ can be found by simply setting $\mathbf{x}_{sp}$ to $\mathbf{e}_2$ (i.e. 0 in all components except for the altitude p_z) and running the simulation for a long time so that the initial transient disappears and all that is left is a periodic oscillation with period Π (see the highlighted curve in Figure 8). An arbitrary point of the periodic orbit, $\mathbf{x}_\Pi(0)$, is then used as a base initial condition; a set of n simulations on the time interval $t \in [0, \Pi]$ was then run with initial conditions $\mathbf{x}_\Pi^{(i)}(0) = \mathbf{x}_\Pi(0) + \epsilon|x_i|\mathbf{e}_i$, (with $|x_i|$ being the amplitude range of x_i over one period of the periodic orbit, i.e. $|x_i| = \left|\max_{t\in[0,\Pi]} x_i(t) - \min_{t\in[0,\Pi]} x_i(t)\right|$), with a numerical value of $\epsilon = 0.1$. The results of those simulations can be seen in Figure 8. The state after one period, $\mathbf{x}_\Pi^{(i)}(0)$, was then used to compute the monodromy matrix $\boldsymbol{\mathcal{M}}$ as indicated in (11) (taking into account the $|x_i|$ factor). The magnitudes of the eigenvalues of $\boldsymbol{\mathcal{M}}$ were all below 1, as shown in Figure 9, therefore proving the stability of the rocket in hover.

Another added value of the Floquet framework is the possibility of evaluating the influence of ν on system performance, since the mean dynamics give little insight into this matter due to their underlying assumption that ν is sufficiently high, while in practice actuator bandwidths provide restrictive ceilings on its values. In contrast, Floquet analysis remains accurate for any periodic motion, whether slow or fast. Since a magnitude of 1 is the limit of stability for Floquet eigenvalues, the highest magnitude among the eigenvalues can be used as a measure of the closed-loop robustness of the system. Repeating the

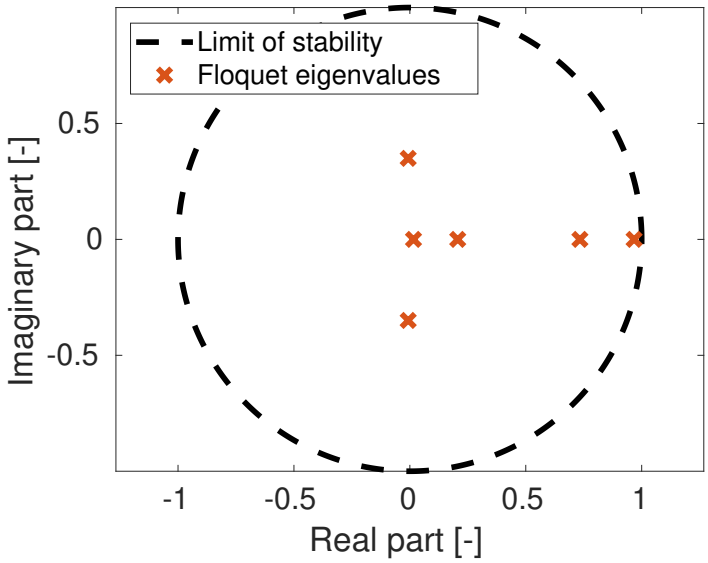

Fig. 9 Discrete Floquet eigenvalues of the closed-loop system with $\nu = 3$ [Hz].

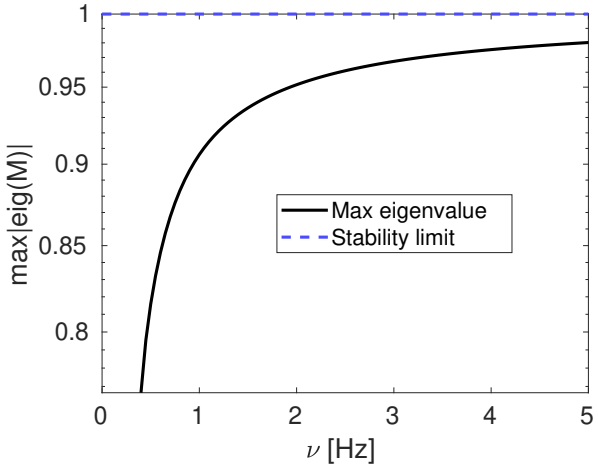

Fig. 10 Maximum magnitude of the eigenvalues of $\mathcal{M}$ as a function of TVC oscillation frequency.

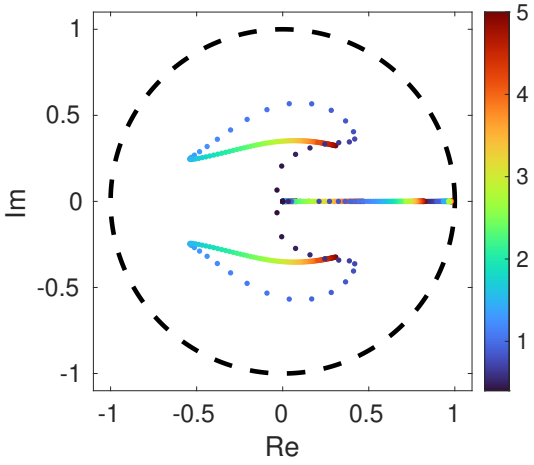

Fig. 11 Root locus of $\mathcal{M}$ (colormap stands for ν values in [Hz]).

Floquet analysis for different values of , one obtains Figure 11. It is worth noting that the system does not seem to have periodic orbits for $\nu < 0.37$ [Hz]; this is not due to an onset of instability in the Floquet sense, since the magnitudes of the eigenvalues at $\nu \approx 0.37$ [Hz] are nowhere near 1. For a clearer picture, Figure 10 shows a plot of the maximum eigenvalue magnitude for different frequencies, showing that in the range of interest anything above $\nu = 0.37$ makes the system stable with some robustness margin.

4 Conclusions

Reusable rockets and landers have been shown to be fully locally controllable using TVC only (assuming that the thrust-to-weight ratio $\frac{T}{m\gamma}$ is in the interval $(1, 2/(1 + \cos\Delta_{\max}))$ using Lie bracket analysis. It was shown that this controllability can be realized by modulating the mean thrust T using open-loop sinusoidal oscillatory TVC actuation, with no side effects appearing in the average dynamics. A linear state feedback controller exploiting the mean thrust modulation to stabilize the system was proposed, along with a derivation of the average closed-loop dynamics. A numerical case study of a landing rocket based on [7] was performed, with the linear state feedback tuned using LQR synthesis. The resulting system was shown to be stable in two ways: by computing the linearized state transition matrix of the average closed-loop dynamics and the monodromy matrix of the full nonlinear time-dependent system in hover; both methods yielded stable eigenvalues. Simultaneous controllability of the horizontal and vertical axes along with good practical performance was demonstrated in an example landing maneuver. The case study also emphasized that despite the control synthesis being performed on the averaged system, which is guaranteed to be accurate only for high TVC oscillation frequencies, the proposed control law displayed good performance and some level of robustness for values of ν of the order of a few Hz. By introducing an actuator model, it was shown that the control architecture can handle at least some forms of unmodeled dynamics, with a possible need to adjust ν to the real system.

While it is definitely preferable for reusable rockets to have throttling control, since the oscillatory TVC approach leaves absolutely no redundancy and might face practical problems due to TVC actuator bandwidths (especially for large spacecraft) and structural vibrations, it is nevertheless useful as a redundancy measure in the event of throttling malfunction, and together with trajectory generation methods such as [7, 8] it might enable the application of solid rocket propulsion for light low-cost landers used e.g. for cargo delivery. Multiple areas for future research were identified during the writing of this paper:

- It should be possible to find some analytical sufficient or necessary conditions on the stability of the average closed-loop dynamics, either using the Lyapunov theorem with the full nonlinear dynamics (48) or applying the Routh-Hurwitz criterion on the linearized system (54); initial attempts by the authors were inconclusive at the time of writing of this paper.
- It could be of interest to check if the sinusoidal TVC oscillation proposed in this paper is a rigorous implementation of movement along the $[[\tilde{\mathbf{f}}, \tilde{\mathbf{g}}_{\hat{\delta}}], \tilde{\mathbf{g}}_{\hat{\delta}}]$ Lie bracket identified in (19) to be the source of z-axis controllability (see [11, 12] for examples of generating motion in the direction of Lie brackets based on theory rather than physical intuition, as was the case in this paper) – and, if this is not the case, to propose an alternative open-loop control law which implements it.
- An analysis of the linearized dynamics of the system could provide some new insights into the choice of ω, since from the linear point of view some frequencies should result in higher $\mathbf{x}$ oscillations (which are an undesirable side effect and should be minimized) than others.
- Since the current control law suffered from a slight static error in p_z when maintaining hover (not highlighted in the paper), an integral term might be added if the application demands it, with the typical drawbacks of integral control (degraded robustness, windup issues etc).
- To further evaluate the feasibility of oscillatory TVC in practical applications, it could be useful to analyze the effect of structural flexibility [22], sloshing [22, 23], or even unsteady aerodynamic effects on the closed-loop performance, along with case studies using numerical data coming from

large reusable launchers rather than scaled models, like the one used in this paper. The findings in subsection 3.2 suggest that the system is capable of handling some degree of unmodeled dynamics, but the TVC oscillation frequency needs to be tailored to them.
- A study of the robustness of the control scheme to parametric uncertainty could provide more practical insights into its limitations.
- To further explore the practical implementability of the control scheme, an experimental study on a scaled platform, such as the one in [7] (which was the source of data for the numerical study in section 3) would be beneficial.

Declaration of Use of Artificial Intelligence

Artificial intelligence was not used in the work presented.

References

[1] Erin Betts and Robert Frederick. A Historical Systems Study of Liquid Rocket Engine Throttling Capabilities. In *46th AIAA/ASME/SAE/ASEE Joint Propulsion Conference & Exhibit*. American Institute of Aeronautics and Astronautics, 2012. doi: 10.2514/6.2010-6541.

[2] Dawid Cieśliński, Adam Okniński, Michał Ranachowski, Marcin Molik, Bartosz Bartkowiak, Krzysztof Matysek, Krystian Kutnik, Aleksander Gorgeri, Grzegorz Ogórek, and Maciej Borys. On development of green storable liquid rocket engine with thrust variation. *Acta Astronautica*, 234:560–574, Sept. 2025. ISSN: 0094-5765. doi: 10.1016/j.actaastro.2025.05.020.

[3] Bonnie Birckenstaedt, Josh Hopkins, Bernard Kutter, Frank Zegler, and Todd Mosher. Lunar Lander Configurations Incorporating Accessibility, Mobility, and Centaur Cryogenic Propulsion Experience. In *Space 2006*, AIAA SPACE Forum. American Institute of Aeronautics and Astronautics, Sept. 2006. doi: 10.2514/6.2006-7284.

[4] Pedro Simplício, Andrés Marcos, and Samir Bennani. Guidance of Reusable Launchers: Improving Descent and Landing Performance. *Journal of Guidance, Control, and Dynamics*, 42(10):2206–2219, 2019. ISSN: 0731-5090. doi: 10.2514/1.G004155.

[5] Daniel Dueri, Behçet Açıkmeşe, Daniel P. Scharf, and Matthew W. Harris. Customized Real-Time Interior-Point Methods for Onboard Powered-Descent Guidance. *Journal of Guidance, Control, and Dynamics*, 40(2):197–212, Feb. 2017. ISSN: 0731-5090, 1533-3884. doi: 10.2514/1.G001480.

[6] Michael Szmuk, Behcet Acikmese, and Andrew W. Berning. Successive Convexification for Fuel-Optimal Powered Landing with Aerodynamic Drag and Non-Convex Constraints. In *AIAA Guidance, Navigation, and Control Conference*, San Diego, California, USA, Jan. 2016. American Institute of Aeronautics and Astronautics. ISBN: 978-1-62410-389-6. doi: 10.2514/6.2016-0378, `https://arc.aiaa.org/doi/10.2514/6.2016-0378`.

[7] Nicolas Bourliatoux, Joan M. Riera, and Leandro R. Lustosa. Definition of a Landing Strategy for a Model-Scale Reusable Rocket. May 2022. doi: 10.82124/CEAS-GNC-2024-041.

[8] Alejandro Tevera-Ruiz, Rodolfo Garcia-Rodriguez, Vicente Parra-Vega, and Luis Enrique Ramos-Velasco. Q-Learning with the Variable Box Method: A Case Study to Land a Solid Rocket. *Machines*, 11(2):214, Feb. 2023. ISSN: 2075-1702. doi: 10.3390/machines11020214.

[9] Nuo Chen, Shang Liu, Xiang Zhou, and Hong-Bo Zhang. Small Solid-Model Rocket Design and Soft Landing Trajectory Planning. *Journal of Spacecraft and Rockets*, 61(6):1667–1679, 2024. ISSN: 0022-4650. doi: 10.2514/1.A35919.

[10] Francesco Bullo and Andrew D Lewis. *Geometric Control of Mechanical Systems: Modeling, Analysis, and Design for Simple Mechanical Control Systems*, volume 49. Springer Science & Business Media, 2004.

[11] Haithem E. Taha, Ahmed Hassan, and Moatasem Fouda. Nonlinear flight physics of the Lie Bracket roll mechanism. *Nonlinear Dynamics*, 106(3):1627–1646, Nov. 2021. ISSN: 1573-269X. doi: 10.1007/s11071-021-06940-z.

[12] Haitham E. Taha. Geometric Nonlinear Control of the Lift Dynamics of a Pitching-Plunging Wing. In *AIAA Scitech 2020 Forum*, AIAA SciTech Forum. American Institute of Aeronautics and Astronautics, Jan. 2020. doi: 10.2514/6.2020-0824.

[13] Ahmed M. Hassan and Haithem E. Taha. Geometric control formulation and nonlinear controllability of airplane flight dynamics. *Nonlinear Dynamics*, 88(4):2651–2669, June 2017. ISSN: 1573-269X. doi: 10.1007/s11071-017-3401-9.

[14] R.M. Murray and S.S. Sastry. Nonholonomic motion planning: steering using sinusoids. *IEEE Transactions on Automatic Control*, 38(5):700–716, May 1993. ISSN: 1558-2523. doi: 10.1109/9.277235.

[15] Mahmoud A. Abdelgalil, Ahmed Hassan, and Haitham E. Taha. On the Motion Planning and Feedback Stabilization of Nonlinear Systems with Drift. In *AIAA Scitech 2021 Forum*. American Institute of Aeronautics and Astronautics. doi: 10.2514/6.2021-1959.

[16] P. L. Kapitsa. Pendulum with an oscillating pivot point. *Achievements of Physical Sciences*, 44(5):7–20, May 1951. ISSN: 0042-1294. doi: 10.3367/UFNr.0044.195105b.0007.

[17] Haithem E. Taha, Mohammadali Kiani, Tyson L. Hedrick, and Jeremy S. M. Greeter. Vibrational control: A hidden stabilization mechanism in insect flight. *Science Robotics*, 5, Sept. 2020. doi: 10.1126/scirobotics.abb1502.

[18] Ahmed Mohamed Anwar Shalaby. Evaluation of the Performance of a Rocket under Oscillatory Thrust. Master's thesis, California State University, Long Beach, United States – California, 2019.

[19] Marco Maggia, Sameh A. Eisa, and Haithem E. Taha. On higher-order averaging of time-periodic systems: reconciliation of two averaging techniques. *Nonlinear Dynamics*, 99(1):813–836, Jan. 2020. ISSN: 1573-269X. doi: 10.1007/s11071-019-05085-4.

[20] Jan A. Sanders, Ferdinand Verhulst, and James A. Murdock. *Averaging methods in nonlinear dynamical systems*. Number v. 59 in Applied mathematical sciences (Springer-Verlag New York Inc.). Springer, New York, 2nd ed edition, 2007. ISBN: 978-0-387-48918-6.

[21] Andrey Sarychev. Stability criteria for time-periodic systems via high-order averaging techniques. In *Nonlinear control in the year 2000 volume 2*, pages 365–377. Springer, 2007.

[22] Timothy M. Barrows and Jeb S. Orr. *Dynamics and Simulation of Flexible Rockets*. Academic Press, Dec. 2020. ISBN: 978-0-12-819995-4.

[23] JOSE ALFREDO MACES-HERNANDEZ, DAVID SEELBINDER, and STEPHAN THEIL. Modelling and Stability Analysis of Sloshing on Liquid-Propelled Reusable Launch Vehicles. page 17 pages, 2023. doi: 10.13009/EUCASS2023-549.